Photonuclear Data Evaluation of ^{235}U

I. Raškinytė, E. Dupont and D. Ridikas
DSM/DAPNIA/SPhN, CEA-Saclay, F-91191 Gif-sur-Yvette Cedex, France

1 Introduction

Both the development and maintenance of nuclear technologies rely on computer simulations and nuclear data, such as energy-dependent reaction cross sections, energy and angular distributions of reaction products, etc.

Photo-induced reaction cross section data are of importance for a variety of current or emerging applications. Among them are radiation shielding design and radiation transport analysis, influence of photoreactions on neutron balance in innovative reactors, diagnostics and shielding of plasma in fusion reactors, activation analysis, safeguards and inspection technologies, nuclear waste transmutation. Most of these applications need evaluated cross sections and emission spectra for transport calculations. In terms of incident energies, the giant dipole resonance region below about $25 - 30$ MeV is essential for most applications. On the other hand, photonuclear data up to energies of approximately 50 MeV are useful for some medical applications. Additionally, it is also desirable to have evaluated photonuclear data up to 130 MeV for the computer simulation of intense neutron sources and to complement the neutron and proton high-energy libraries.

Measurements of delayed neutron yields on ^{238}U and ^{232}Th nuclei have been performed by DSM/DAPNIA/SPhN and experiments on ^{235}U, ^{237}Np and ^{239}Pu nuclei are planed. In connection with these measurements evaluation of above mentioned nuclei will be performed. These evaluated files will be submitted to the JEFF project and should contain photonuclear reaction cross sections up to 130 MeV, fission yields as well as prompt and delayed neutron yields. Cross sections of ^{232}Th, ^{235,238}U and ^{239}Pu were already evaluated in the framework of a specific IAEA coordinated research project [1]; ^{235,238}U, ^{237}Np and ^{239}Pu were recently evaluated by M.-L. Giacri-Mauborgne *et al.* [2] using the Gnash code. All above mentioned evaluations were done for incident photon energies up to 20 MeV. The objective of this report is to present cross sections calculation up to 130 MeV for ^{235}U using Talys-0.64 [3].

2 Reaction mechanisms

In a photoreaction, the ^{235}U nucleus is excited by the absorption of a photon. When the excitation energy is big enough, the nucleus can emit neutron or undergo fission. The probability to emit charged particles is small for heavy nuclei due to the Coulomb interaction and thus is negligible in present calculations. Residual nucleus can further emit neutron or fission depending on its excitation energy. A schematic representation of the different reaction steps is given in Figure 1.

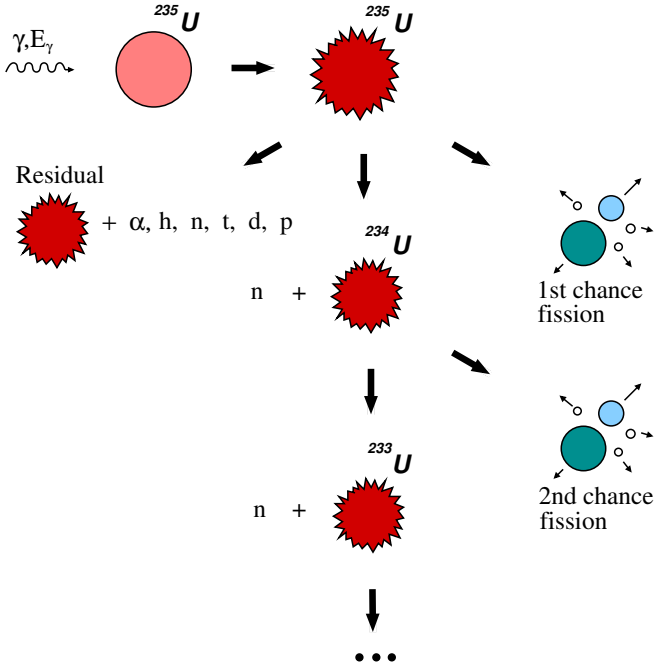

Figure 1: γ+^{235}U decay chain

In this work, the photoabsorption process is described by the giant dipole resonance and quasi deuteron mechanisms, neutron emission is treated within the preequilibrium and statistical models while fission is also calculated within this statistical approach using a double humped fission barrier. The ^{235}U (γ, n), $(\gamma, 2n)$ and (γ, f) cross sections are calculated with the Talys-0.64 code [3], which includes all reaction mechanisms mentioned above.

2.1 Photoabsorption

Photon induced reaction calculations starts with the determination of the photoabsorption cross section. At low energies, below about 30 MeV, the giant dipole resonance (GDR) is the dominant excitation mechanism. At

higher energies, up to 150 MeV, the phenomenological model of photoabsorption on a neutron-proton (quasi-deuteron, QD) becomes important. Following Chadwick *et al.* [4], the photoabsorption cross section is given by

$$\sigma_{abs}(E_\gamma) = \sigma_{GDR}(E_\gamma) + \sigma_{QD}(E_\gamma). \quad (1)$$

In the case of deformed nuclei, the GDR component is given as a sum of two Lorentzians

$$\sigma_{GDR}(E_\gamma) = \sum_{i=1,2} \sigma_{E1,i} \frac{E_\gamma^2 \Gamma_{E1,i}^2}{(E_\gamma^2 - E_{E1,i}^2)^2 + E_\gamma^2 \Gamma_{E1,i}^2}, \quad (2)$$

where $\sigma_{E1,i}$, $E_{E1,i}$, $\Gamma_{E1,i}$ are the GDR peak cross section, energy and width respectively. Parameters used in present calculations are the same as given in Ripl-2 [5] and are derived from fits to experimental data by Caldwell *et al.* [6]. The QD component is taken from the model of Chadwick *et al.* [4]. It relates photoabsorption cross section to the experimental deuteron photodisintegration cross section $\sigma_d(E_\gamma)$ by

$$\sigma_{QD}(E_\gamma) = L \frac{NZ}{A} \sigma_d(E_\gamma) f(E_\gamma), \quad (3)$$

where L is the so called Levinger parameter and $f(E_\gamma)$ is the Pauli blocking function. For more details see reference [4].

None of the default Talys photoabsorption parameters were changed in the present calculation. Figure 2 presents comparison between default Talys photoabsorption cross section and experimental data. Caldwell points are given as the sum of measured (γ, n), $(\gamma, 2n)$ and (γ, f) cross sections. While Gurevich *et al.* [7] directly measured total photoabsorption cross section by the absorption method. The default Talys photoabsorption cross section is described by two Lorentzians fitted to Caldwell data in the energy region between 9 and 18 MeV. Difference between Lorentzians and Caldwell points below 9 MeV is taken into account through γ-ray scattering within Talys statistical model calculations.

2.2 Optical model

For the inverse channels calculations the global coupled-channels optical potential by Soukhovitskii *et al.* [8] was used. This potential was developed for neutron-actinide interaction from 1 keV to 200 MeV. Coupling between levels in coupled-channel calculations is due to the deformed nuclear optical potential, where deformation is taken into account through the deformed nuclear shapes

$$R(\theta', \varphi') = R_0 \left\{ 1 + \sum_{\lambda=2,4,6} \beta_{\lambda 0} Y_{\lambda 0}(\theta', \varphi') \right\}, \quad (4)$$

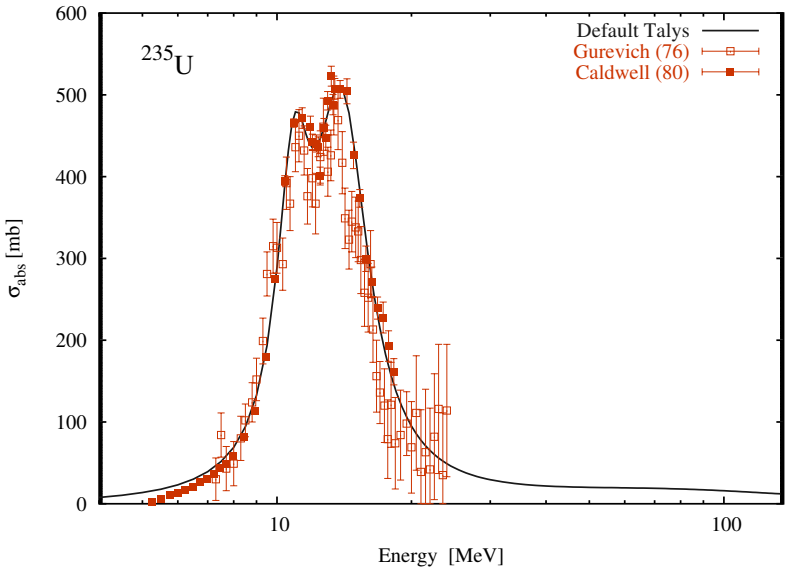

Figure 2: ^{235}U photoabsorption cross section

where $Y_{\lambda 0}$ are spherical harmonics and (θ', φ') are angular coordinates in the body-fixed frame. The optical potential is of a standard Wood-Saxon form with real and imaginary volume, imaginary surface and real and imaginary spin-orbit terms

$$\begin{aligned}
-V_R f_R(r, R(\theta', \varphi')) &\quad \text{real volume (R)} \\
-iW_V f_V(r, R(\theta', \varphi')) &\quad \text{imaginary volume (V)} \\
i4W_D a_D \frac{d}{dr} f_D(r, R(\theta', \varphi')) &\quad \text{imaginary surface (D)} \\
\left(\frac{\hbar}{m_\pi c}\right)^2 V_{so} \frac{1}{r}\frac{d}{dr} f_{so}(r, R(\theta', \varphi'))\hat{\sigma}\cdot\hat{L} &\quad \text{real spin-orbit (so)} \\
i\left(\frac{\hbar}{m_\pi c}\right)^2 W_{so} \frac{1}{r}\frac{d}{dr} f_{so}(r, R(\theta', \varphi'))\hat{\sigma}\cdot\hat{L} &\quad \text{imaginary spin-orbit (so),}
\end{aligned} \tag{5}$$

with the form factors given as

$$f_i(r) = \left[1 + exp((r - R_i(\theta', \varphi'))/a_i)\right]^{-1}, \qquad i = R, V, D, so. \tag{6}$$

Deformed radii R_i are given by equation (4) with $R_0 = r_i A^{1/3}$. Well depths V_i as well as r_R are energy dependent. Their functional dependence as well as values of r_i and a_i were obtained from [8]. The potential parameters were searched for to reproduce available neutron- and proton-induced cross section data for ^{238}U and ^{232}Th. Coupled-channels calculations were performed by coupling the first five states of the ground state rotational band.

All previous parameters except deformation parameters (adjustable) were used to predict cross sections of other actinides like ^{233}U and ^{235}U.

For the inverse ^{234}U+neutron channel we used interpolated deformation parameters between ^{233}U and ^{235}U as given in [8]. The following table summarizes deformation parameter values used for uranium isotopes.

Nuclide	β_{20}	β_{40}	β_{60}	Ref.
^{233}U	0.183	0.120	0.003	[8]
^{234}U	0.190	0.110	0.001	This work
^{235}U	0.198	0.099	−0.0097	[8]
^{238}U	0.223	0.056	−0.0072	[8]

Calculated neutron total cross sections for ^{233}U and ^{234}U nuclei are shown in Figure 3 and 4 and are compared to experimental data.

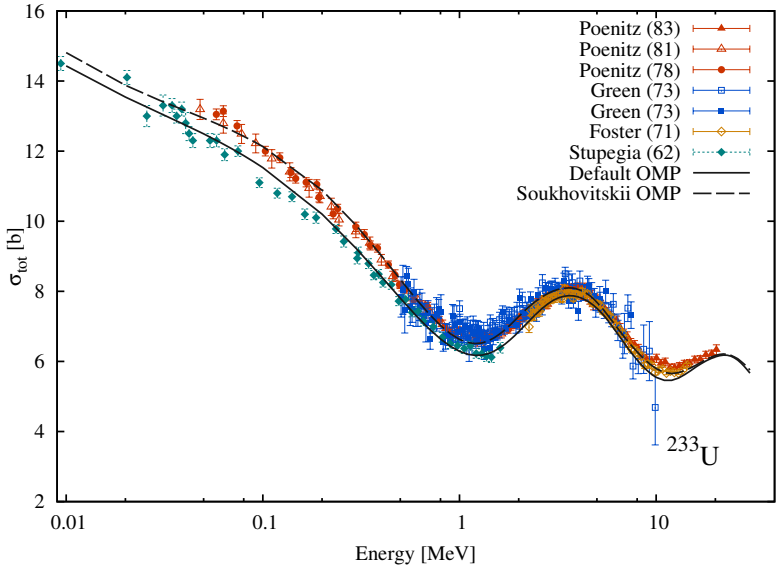

Figure 3: ^{233}U total neutron cross section

All experimental data are taken from the EXFOR library, where there are records for ^{233}U from 0.01 to 30 MeV and no information for ^{234}U. Thus calculated total cross sections of the former nucleus are plotted only up to 30 MeV and total cross sections of the latter are compared to natural uranium data from 0.01 to 130 MeV. For the clarity of the figures some EXFOR entries are not included in the plots. This does not affect the overall interpretation of the results: the agreement between EXFOR and total cross sections obtained with Soukhovitskii *et al.* optical potential is better in the whole energy range compared to the default spherical optical potential calculations initially provided by Talys.

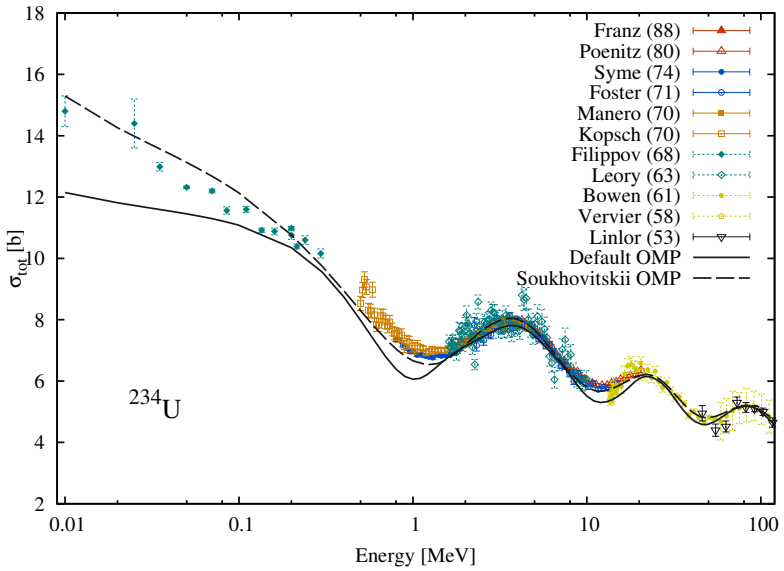

Figure 4: ^{234}U total neutron cross section, experimental data are for ^{nat}U

2.3 Level densities

Total level densities are important ingredients in statistical reaction approach calculations. Talys-0.64 includes several level densities models. Among these models are: Gilbert-Cameron [9], Fermi gas with deformation-dependent collective effects, HF-BCS [5, 10]. At the moment, calculations were done only with Gilbert-Cameron level densities. Calculations with other level densities models will be made in the future to investigate the sensitivity of the results to these parameters.

In the Gilbert and Cameron level density formulation, the excitation energy range is divided in a low energy part from zero to a matching energy E_M and a high energy part from E_M to infinity

$$\rho(E_{ex}) = \begin{cases} \rho_T(E_{ex}), & E_{ex} \leq E_M \\ \rho_F(E_{ex}), & E_{ex} > E_M. \end{cases} \tag{7}$$

At low excitation energy, the model is based on the experimental evidence that the cumulative number of the first discrete levels vs. energy can be well reproduced by a constant temperature law. Accordingly the constant temperature part of the total level densities is

$$\rho_T(E_{ex}) = \frac{1}{T} \exp \frac{E_{ex} - E_0}{T}. \tag{8}$$

The nuclear temperature T and E_0 are adjustable parameters. For higher energies, the Fermi gas model is more suitable and the total level densities

is then given by

$$\rho_F(E_{ex}) = \frac{\pi}{12}\frac{\exp(2\sqrt{(aU)})}{a^{1/4}U^{5/4}}, \tag{9}$$

where $U = E_{ex} - \Delta$ and a is level density parameter. In our calculations we used Ignatyuk [11] level density parameter formula

$$a = \tilde{a}\left[1 + \delta W \frac{1-\exp(-\gamma U)}{U}\right]. \tag{10}$$

In present calculations, pairing energy Δ, asymptotic level density value $\tilde{a}$, shell damping parameter γ and shell correction energy δW are deduced from systematics [3]. The expressions for ρ_T and ρ_F are matched by requiring the continuity of the function $\rho(E_{ex})$ and its derivative at energy E_M. Another constraint is given by considering that in the discrete level region, the constant temperature law should reproduce the experimental discrete levels from a lower level N_{low} to an upper level N_{top}. That is the levels N_{low} and N_{top} should be chosen such that $\rho_T(E_{ex})$ optimally describes the observed discrete states. In default Talys calculations N_{low} equal 2 and N_{top} is determined from microscopic level densities.

Comparison between default Talys level densities and the one used in our calculations for ^{233}U, ^{234}U and ^{235}U are given in Figure 5, 6 and 7.

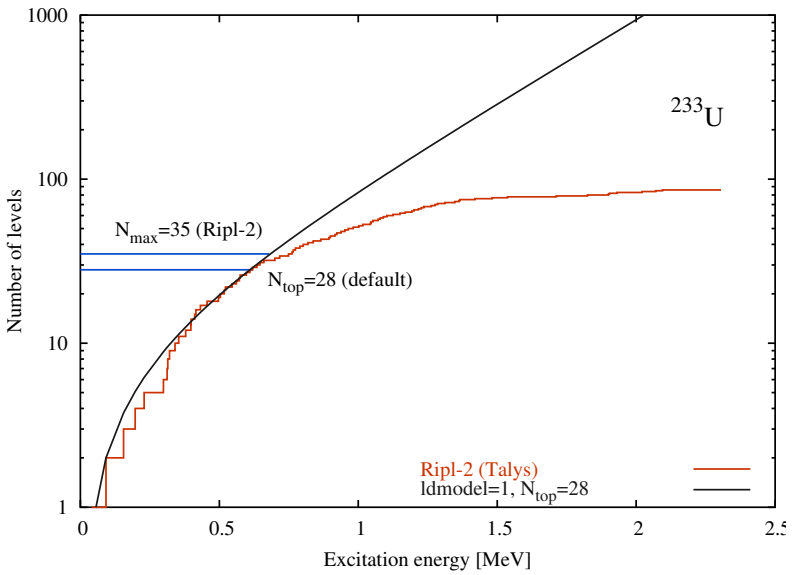

Figure 5: Number of levels vs. energy in ^{233}U

For the ^{233}U nucleus we used default level densities values. For ^{234}U isotope, N_{top} was changed from 30 to 40 in order to better reproduce the

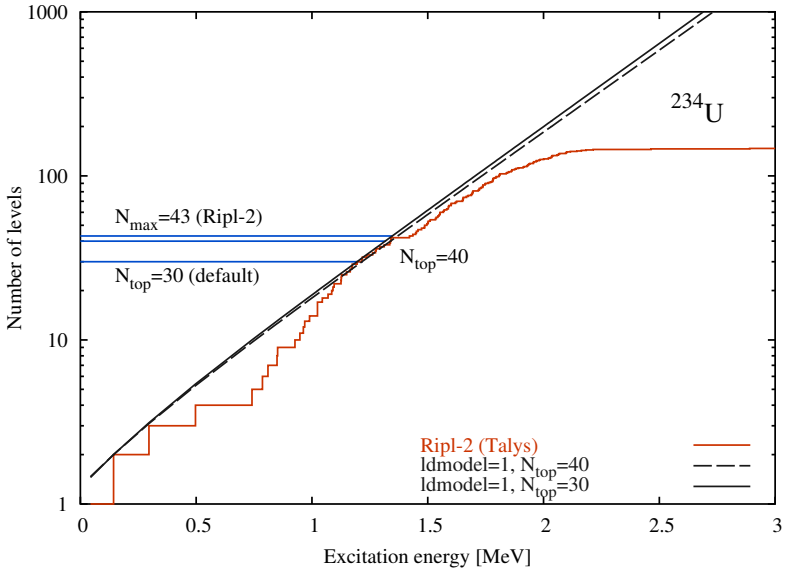

Figure 6: Number of levels vs. energy in ^{234}U

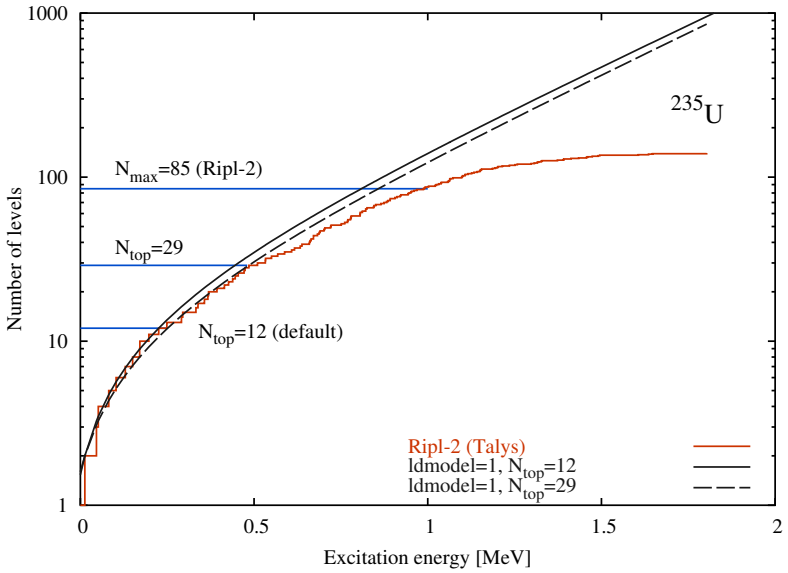

Figure 7: Number of levels vs. energy in ^{235}U

number of experimental levels in the energy region between 1 and 1.5 MeV. For the ^{235}U nucleus, N_{top} was changed from the default value 12 to 29. It led to a slight decrease of the total level density.

2.4 Fission

The compound nucleus, when its excitation energy is large enough, can emit gamma rays, particles or may fission. Usually the fission process is accounted for through a statistical model approach. For present calculations, fission transmission coefficients were calculated using a double humped barrier model. The Hill-Wheeler expression gives the quantum penetrability through a fission barrier described by an inverted parabola, which reads

$$T_{HW}(E_{ex}) = \left[1 + exp\left(-2\pi\frac{E_{ex} - B_f}{\hbar\omega}\right)\right]^{-1}, \tag{11}$$

where B_f is the barrier height relative to the nucleus ground state and $\hbar\omega$ is the barrier curvature. For a transition state with excitation energy ϵ_i above the top of the same barrier, one has

$$T_{HW}(E_{ex}, \epsilon_i) = \left[1 + exp\left(-2\pi\frac{E_{ex} - B_f - \epsilon_i}{\hbar\omega}\right)\right]^{-1} \tag{12}$$

which means that the barrier is simply shifted up by ϵ_i. For a compound nucleus with excitation energy E_{ex}, spin J, and parity Π, the total fission transmission coefficient is the sum of the individual transmission coefficients for each barrier through which the nucleus may tunnel

$$T_f^{J,\Pi}(E_{ex}) = \sum_i T_{HW}(E_{ex}, \epsilon_i) f(i, J, \Pi) + \int_{E_{th}}^{E_{ex}} \rho(\epsilon, J, \Pi) T_{HW}(E_{ex}, \epsilon) d\epsilon. \tag{13}$$

The summation runs over all discrete transition states on top of the barrier and E_{th} marks the beginning of the continuum. $f(i, J, \Pi) = 1$, if the spin and parity of the transition state equal that of the compound nucleus and 0 otherwise. Moreover, $\rho(\epsilon, J, \Pi)$ are the level densities of fission channels with spin J and parity Π for an excitation energy ϵ.

In the case of a double humped barrier one first calculates the first barrier (A) and the second barrier (B) fission transmission coefficients $T_A^{J\Pi}$ and $T_B^{J\Pi}$. Then one assumes that tunneling through two barriers can be separated into two steps. One first should know the probability to cross the first barrier and then multiply it by the probability to fission. Consequently the effective fission transmission coefficient is given as

$$T_{eff}^{J\Pi} = \frac{T_A^{J\Pi} T_B^{J\Pi}}{T_A^{J\Pi} + T_B^{J\Pi}}. \tag{14}$$

The only fission parameters changed in present calculations are fission barrier heights and widths. The two tables below list default Talys values which corresponds to Ripl-2 data [5] together with the ones used in this work.

Default

	B_{f1}	$\hbar\omega_{f1}$	B_{f2}	$\hbar\omega_{f2}$
^{235}U	5.25	0.7	6.0	0.5
^{234}U	4.80	0.9	5.5	0.6

This work

	B_{f1}	$\hbar\omega_{f1}$	B_{f2}	$\hbar\omega_{f2}$
^{235}U	5.25	0.7	7.07	1.5
^{234}U	6.34	1.2	5.5	0.8

3 Calculations and results

Here we present calculations done for the ^{235}U nucleus up to now. Figure 8 shows comparison between default Talys calculations using the models and their parameters intrinsically defined in the code and calculations performed with global coupled-channels optical potential by Soukhovitskii *et al.* [8].

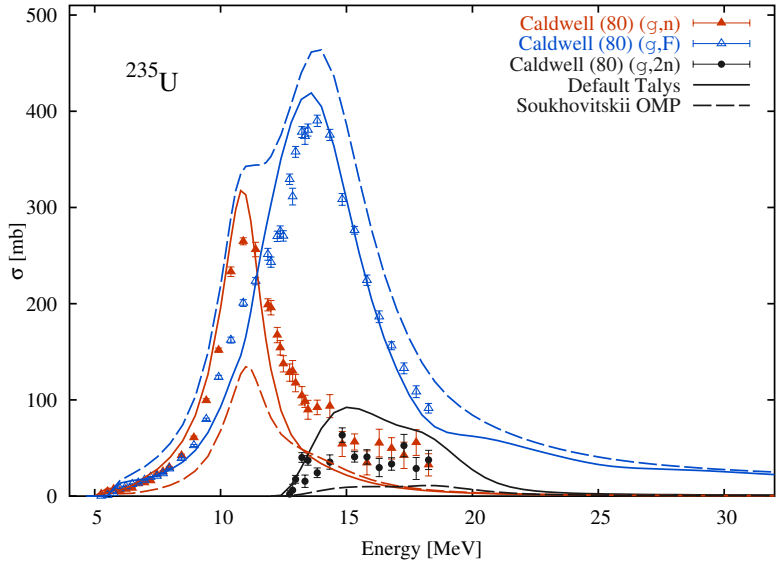

Figure 8: ^{235}U (γ, n), $(\gamma, 2n)$ and (γ, f) cross sections with default Talys and Soukhovitskii *et al.* [8] optical potentials

In our calculations we used only the first three states of the ground state rotational band together with unaltered optical potential parameters. Coupling the first three levels (vs. five levels) alters for example the total cross section at energies below 0.2 MeV, yet influence on (γ, n), $(\gamma, 2n)$ and (γ, f) cross sections is negligible. In addition ^{234}U+neutron transmission coefficients were also used for ^{233}U+neutron exit channel. This approximation does not affect significantly the calculated cross sections. In Figure 8, default calculations and calculations done with the new optical potential are given as solid and dashed lines respectively. As one can see (γ, n), $(\gamma, 2n)$ and (γ, f) cross sections are all sensitive to the optical potential.

Afterwards, calculations were done with and without adapted ^{233}U, ^{234}U and ^{235}U level densities as presented in Figure 5, 6 and 7 together with the new optical potential. Changes in level densities have no visible effect on calculated cross sections.

Finally, number of runs were done in order to find a set of fission parameters which reproduce Caldwell *et al.* [6] experimental data. The only fission parameters changed are fission barrier heights and widths. Parameters found in this work are listed in subsection 2.4. Cross sections obtained using default and adjusted fission parameters together with the new optical model are plotted in Figure 9. By adjusting barrier heights and widths we were able to reproduce all cross sections.

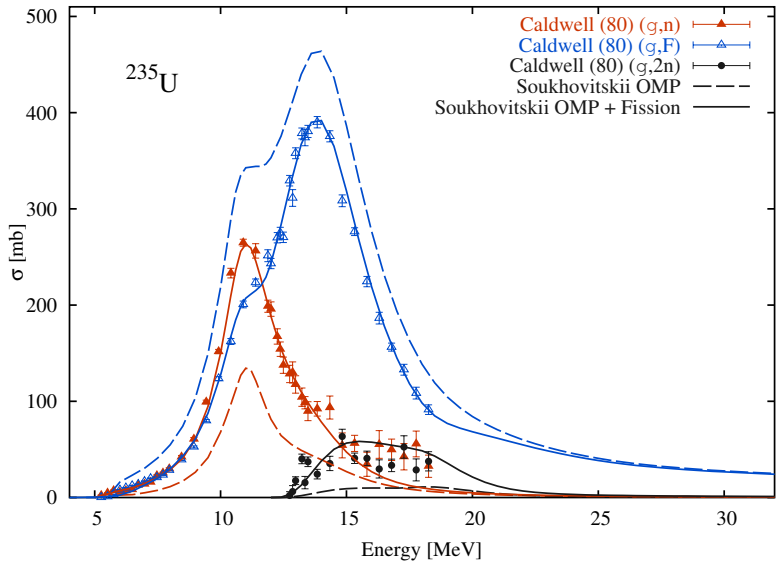

Figure 9: ^{235}U (γ, n), $(\gamma, 2n)$ and (γ, f) cross sections using Soukhovitskii *et al.* [8] optical potential with default Talys and adjusted fission parameters

Figure 10 presents final results with calculations extended to 130 MeV. Only fission data are available at high energy in the EXFOR database. These data are well reproduced by the quasi deuteron model. We plotted besides Caldwell data other fission measurements together with Varlamov evaluation. Our calculated total fission cross section is above Varlamov points. In order to reproduce them one would need to alter the selected absorption cross section based on Caldwell *et al.* data [6].

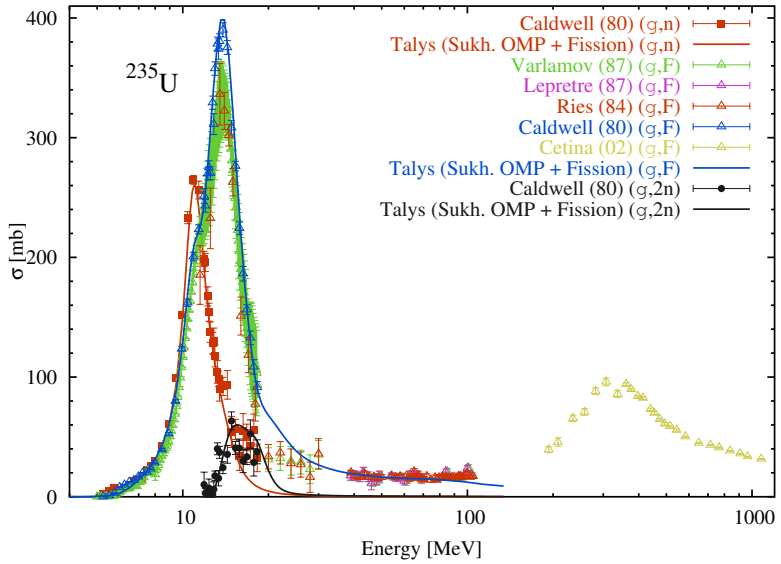

Figure 10: ^{235}U (γ, n), $(\gamma, 2n)$ and (γ, f) cross sections up to 130 MeV.

4 Conclusions

^{235}U (γ, n), $(\gamma, 2n)$ and (γ, f) cross sections up to 130 MeV were calculated with Talys-0.64 using a coupled-channels optical potential by Soukhovitskii *et al.*. Changes in level densities did not affect results significantly. The fission transmission coefficients were calculated using a double humped barrier model. Fission barriers heights and widths were modified to reproduce experimental data. Neither fission level densities nor other default fission parameters were changed. More calculations are needed in order to check cross sections sensitivity to other level densities and fission models. Eventually, the results will be transformed into the ENDF format and proposed to the JEFF project. This work will continue in collaboration with the nuclear physics group from Bruyères-le-châtel (DAM/DPTA/SPN).

References

[1] M. B. Chadwick, P. Oblozinsky, A. I. Blokhin, T. Fukahori, Y. Han, Y.-O. Lee, M. N. Martins, S. F. Mughabghab, V. V. Varlamov, B. Yu, and J. Zhang. IAEA-TECDOC-1178, Vienna, http://www-nds.iaea.org/photonuclear/. 2000.

[2] M.-L. Giacri-Mauborgne, D. Ridikas, M. B. Chadwick, P. G. Young, and W. B. Wilson. *Nucl. Sci. Eng.*, 153:33, 2006.

[3] A. J. Koning, S. Hilaire, and M. C. Duijvestijn. *Proc. of the Int. Conference on Nuclear Data for Sciece and Technology (ND2004).*

[4] M. B. Chadwick, P. Oblozinsky, P. E. Hodgson, and G. Reffo. *Phys. Rev. C*, 44:814, 1991.

[5] IAEA-CRP, Reference Input Parameter Library (RIPL), IAEA-TECDOC-1034, Vienna, http://www-nds.iaea.org/ripl/. 1998.

[6] J. T. Caldwell, E. J. Dowdy, B. L. Berman, R. A. Alvarez, and P. Meyer. *Phys. Rev. C*, 21:1215, 1980.

[7] G. M. Gurevich, L. E. Lazareva, V. M. Mazur, G. V. Solodukhov, and B. A. Tulupov. *Nucl. Phys. A*, 273:326, 1976.

[8] E. Sh. Soukhovitskii, S. Chiba, J. Lee, O. Iwamoto, and T. Fukahori. *J. Phys. G: Nucl. Part. Phys.*, 30:905, 2004.

[9] A. Gilbert and A. G. W. Cameron. *Can. J. Phys.*, 43:1446, 1965.

[10] P. Demetriou and S. Goriely. *Nucl. Phys. A*, 695:95, 2001.

[11] A. V. Ignatyuk, G. N. Smirenkin, and A. S. Tishin. *Sov. J. Nucl. Phys.*, 21:255, 1975.